

# Spurious internal wave generation during data assimilation in eddy resolving ocean model simulations

Keshav J. Raja<sup>a,b,\*</sup>, Maarten C. Buijsman<sup>b</sup>, Alexandra Bozec<sup>a</sup>, Robert W. Helber<sup>c</sup>, Jay F. Shriver<sup>c</sup>, Alan Wallcraft<sup>a</sup>, Eric P. Chassignet<sup>a</sup>, Brian K. Arbic<sup>d</sup>

<sup>a</sup> Center for Ocean-Atmospheric Prediction Studies, Florida State University, Tallahassee, FL, United States of America

<sup>b</sup> School of Ocean Science and Engineering, University of Southern Mississippi, Stennis Space Center, MS, United States of America

<sup>c</sup> Ocean Dynamics and Prediction Branch, Naval Research Laboratory, Stennis Space Center, MS, United States of America

<sup>d</sup> Department of Earth and Environmental Sciences, University of Michigan, Ann Arbor, MI, United States of America

## ARTICLE INFO

### Keywords:

Data assimilation

Near-inertial waves

Hybrid coordinate ocean model

## ABSTRACT

Data assimilation (DA) combines observational data and the dynamical ocean model to forecast the ocean state in a manner that is not possible from either observations or models by themselves. However, the incorporation of data-derived corrections into the model introduces the potential to disrupt the dynamical balance of the model state, leading to initialization shocks. These shocks arise as the model undergoes a process of adjustment to restore the perturbed dynamic balance, involving the generation of spurious near-inertial motions. Notably, the US Navy's global ocean forecast system strives to mitigate these issues through the implementation of the Incremental Analysis Update (IAU) method, distributing the DA corrections to the model state across a specified time window (3 h in the operational system). Our study shows that, despite the implementation of this 3 h IAU period, the initialization shocks still persist in the model analysis fields. We find that during DA updates, spurious internal waves are generated that are in a broad near-inertial frequency range and propagate long distances from their generation sites in the form of low-mode near-inertial waves. The depth-integrated, time-mean near-inertial kinetic energy in a simulation with DA is 68% higher than in a corresponding forward simulation (free-run, without DA) of the simulation with the same surface wind forcing. The presence of these spurious near-inertial waves disrupts the ocean model energetics, and minimizing them is crucial for using the assimilative model simulations to study small scale/high-frequency ocean dynamics. We also examine a possible way to minimize the spurious internal waves by extending the IAU period in numerical experiments using regional model simulations. We demonstrate that the generation of spurious near-inertial waves can be minimized if we insert increments of smaller magnitude at each time step during the update, which can be achieved by extending the IAU period. Our findings indicate that in simulations with a 24 h IAU period, the variance of near-inertial kinetic energy between the assimilative and forward simulations is reduced to approximately 1%.

## 1. Introduction

The Global Ocean Forecast System (GOFS), the U.S. Navy's operational global ocean prediction system, runs daily at US Navy production centers. The system offers the Fleet accurate 3-dimensional fields of ocean temperature, salinity, and current structure as well as the location of mesoscale oceanic eddies and fronts. The current operational version of GOFS, version 3.1 (Chassignet et al., 2009; Metzger et al., 2017), relies on the Hybrid Coordinate Ocean Model (HYCOM) (Bleck, 2002; Chassignet et al., 2003) coupled with the Community Ice Code version 4 (CICE4) (Hunke and Lipscomb, 2008). Over time, GOFS has improved its predictive capabilities for ocean circulation over a wide

range of spatio-temporal scales. The assimilation of observational data using the Navy Coupled Ocean Data Assimilation (NCODA) system, a three-dimensional variational DA technique, has significantly lowered the forecast errors of sub-tidal fields (Chassignet et al., 2009; Cummings and Peak, 2014). These accomplishments of GOFS 3.1 have motivated the Navy to develop GOFS 3.5 that includes tidal forcing in a higher resolution ocean model (1/25° HYCOM) (Metzger et al., 2020).

In the last decade, the non-assimilative, high-resolution, global HYCOM with tides has demonstrated accurate representation of barotropic and internal tides compared to observations (Arbic et al., 2010, 2012, 2018; Shriver et al., 2012; Buijsman et al., 2020; Arbic, 2022). The

\* Corresponding author at: Center for Ocean-Atmospheric Prediction Studies, Florida State University, Tallahassee, FL, United States of America.

E-mail address: [kraja@fsu.edu](mailto:kraja@fsu.edu) (K.J. Raja).

<https://doi.org/10.1016/j.ocemod.2024.102340>

Received 14 April 2023; Received in revised form 2 February 2024; Accepted 9 February 2024

Available online 10 February 2024

1463-5003/© 2024 The Authors. Published by Elsevier Ltd. This is an open access article under the CC BY-NC-ND license (<http://creativecommons.org/licenses/by-nc-nd/4.0/>).

simultaneous inclusion of tidal and atmospheric forcing in HYCOM simulations has shown to produce a partially resolved super-tidal internal gravity wave continuum (Müller et al., 2015; Savage et al., 2017a) and a geographical distribution of non-phase-locked internal tides (Shriver et al., 2014; Buijsman et al., 2017; Savage et al., 2017b) that agrees with inferences from altimetry (Nelson et al., 2019). It is therefore expected that with the addition of data assimilation, high-resolution HYCOM simulations with tides will be able to accurately predict the amplitudes and phases of the non-phase-locked internal tides. This would make the assimilative HYCOM an ideal candidate to be used as an internal tide correction model for next generation altimeter missions such as the Surface Water Ocean Topography (SWOT) mission (Morrow et al., 2019).

However, the current implementation of DA in the high-resolution HYCOM simulations is not without drawbacks. As with many intermittent DA methods, the addition of data-derived corrections to the model background fields in NCODA is prone to perturb the dynamical balance of the analysis state (see Section 3.1), and causes initialization shocks. These shocks are generated when the model undergoes a process of adjustment to regain the lost dynamic balance. In an attempt to minimize these issues, the HYCOM-NCODA system implements a method called Incremental Analysis Update (IAU) that distributes the DA corrections to the model states over a specified time window (3 h in the operational system).

The IAU method introduced by Bloom et al. (1996) was originally developed as an initialization procedure for three-dimensional atmospheric DA systems. The IAU has since been incorporated into ocean forecast systems that use intermittent DA methods, and has found some notable success in minimizing the initialization shocks during updates (Ourmières et al., 2006). The IAU process incorporates analysis increments, calculated by the DA system, into a model in a gradual manner by using the increments as constant forcings in the model's prognostic equations over a period of time, i.e. the IAU period, centered on an analysis time. The expectation is that the extent of the dynamical imbalance in the analysis field could potentially be reduced by introducing smaller increments at each time step during the IAU period. However, a detailed investigation into the effectiveness of the IAU method in HYCOM-NCODA was never carried out, to the best of our knowledge.

In this paper, we show that, the initialization shocks still persist in the high-resolution HYCOM forecast system (GOF3.5) in spite of implementing a 3 h IAU period. Past literature investigating the issue of DA induced model imbalances have focused on local (non-propagating) noise and the impact of this noise on the representation of mesoscale eddies (Lange et al., 2017; Waters et al., 2017; Pilo et al., 2018; Gasparin et al., 2021). We find that analyzing the near-inertial frequency range in the model output fields reveals the presence of spurious internal waves. The generation and propagation of spurious near-inertial waves (NIWs) in assimilative ocean model simulations has never been explicitly investigated before, to the best of our knowledge. The presence of these spurious waves that can propagate long distances from their generation sites can severely impact the ocean energetics in the model and render the assimilative simulations much less useful for studying small-scale or high-frequency ocean dynamics. We also examine a possible way to minimize the generation of spurious internal waves through the use of extended IAU periods.

The layout of this paper is as follows. In Section 2, we describe the model setup and the analytical methods we use in the paper. The results from our analyses of the global ocean model simulations are discussed in Section 3. We use a global HYCOM simulation coupled with NCODA to present the problem of model adjustment and characterize the spurious NIWs in the model output. The assimilative simulation is compared against a forward simulation, run with the same forcing over the same time period. In Section 4, we analyze the impact of the duration of IAU period on the generation of spurious NIWs using regional simulations of HYCOM. Finally, a summary and discussion of our findings are presented in Section 5.

## 2. Model configuration and analysis methods

### 2.1. Ocean model simulations

The two global HYCOM simulations — one with DA (EXPT 21.6), and the other with no DA (EXPT 19.0), are run on a tri-polar grid at  $1/25^\circ$  horizontal resolution ( $\sim 3\text{--}4$  km in mid-latitudes) and 41 vertical layers. The DA in EXPT 21.6 is provided by the NCODA system with a 24 h observation window. NCODA uses a 24 h HYCOM forecast as a first guess (background fields) in a 3D variational (3DVAR) scheme and increments are computed at the measurement times within the observation window by comparing the observations against time-dependent background fields using the First-Guess at Appropriate Time (FGAT) method (Metzger et al., 2020). A 24 h running average is used to remove most of the tidal signals from the background fields before employing the FGAT technique. The data assimilated include available satellite altimeter observations, satellite and in-situ Sea Surface Temperature (SST) as well as available temperature and salinity profiles from expendable bathythermographs (XBTs), Argo floats and moored buoys (Metzger et al., 2020). Geostrophic balanced increments of velocities are generated using multivariate correlations with the geopotential increments, which are in hydrostatic agreement with the temperature and salinity increments (Cummings and Smedstad, 2014). The data-derived increments are inserted into the background fields over a 3 h IAU period to generate the analysis fields.

The global simulations have realistic atmospheric forcing from the Navy Global Environmental Model (NAVEM) (Hogan et al., 2014) with 60 atmospheric levels over a height of 19 km and a horizontal resolution of  $0.17^\circ$ . The atmospheric forcing is applied every 3 h. HYCOM uses relative winds over the ocean surface to calculate the surface wind stress. The tidal forcing in the simulations includes the  $M_2$ ,  $S_2$ ,  $K_1$ ,  $O_1$ , and  $N_2$  tidal constituents. The HYCOM simulations use a  $K$ -profile parameterization (KPP) scheme as the subgrid scale vertical mixing model. In this paper, we diagnose the hourly model output data from May 20, 2019 to June 19, 2019 (30 days). The non-DA (forward) simulation, EXPT 19.0, is a twin of EXPT 21.6 with the DA turned off on April 1, 2019 (50 days before the analysis period), providing enough time for the model to reach a steady state.

We also run HYCOM simulations in a regional configuration in the Gulf of Mexico varying different model parameters (wind forcing, tidal forcing, IAU period), to study the spurious NIWs in isolation from the wind-driven NIWs in the region, and test the effect of IAU period on the generation of the spurious NIWs. The regional simulations are discussed in detail in Section 4.

### 2.2. Analysis methods

#### 2.2.1. Rotary velocity spectra

The rotary spectra analysis is a technique to decompose a vector time series into clockwise and counter-clockwise components. The separation of a velocity vector into oppositely rotating components can reveal important aspects of the wave field at the specified frequencies (e.g., Yu et al., 2019). The method has proven especially useful for investigating wind-generated inertial motions, currents over abrupt topography, diurnal frequency continental shelf waves, and other forms of narrow-band oscillatory flow (Gonella, 1972; Leaman and Sanford, 1975). In many cases, one of the rotary components (typically, the clockwise component in the northern hemisphere and counter-clockwise component in the southern hemisphere) dominates the currents so that we need to deal with only one scalar quantity rather than two. For example, inertial oscillations rotate almost entirely clockwise (counterclockwise) in the northern (southern) hemisphere so that the counter-clockwise (clockwise) component may be ignored. The clockwise spectra are usually defined for negative frequencies and counterclockwise spectra for positive frequencies (Thomson and Emery, 2014).

In our analysis, the rotary spectra are computed, following methods in Thomson and Emery (2014), from model horizontal velocity vectors. We first compute the 1-dimensional discrete Fourier transform of complex-valued velocity. The clockwise and counter-clockwise rotary spectra are formed by the one-sided autospectra and the quadrature spectra, calculated by multiplying the Fourier coefficients by their complex conjugates. The surface velocity rotary spectra are zonally averaged over  $0.5^\circ$  latitude bins.

### 2.2.2. Near-inertial wave (NIW) energetics

The near-inertial fields are obtained from the model output using the filter method described in Raja et al. (2022). The phase-locked tides are removed from the model output fields using a harmonic analysis and a bandpass filter is applied with frequency limits  $0.8f - 1/13.21$  h equatorwards of  $56^\circ$  and  $[0.8 - 1.2]f$  polewards of  $\pm 56^\circ$ . The frequency band is designed in such a way that semidiurnal internal tides that are generated poleward of  $56^\circ$  and propagate equatorward are removed. This allows us to capture NIWs that have propagated a large distance from their generation sites.

We use the filtered near-inertial fields to calculate the near-inertial surface wind power input,  $W$  as

$$W = \boldsymbol{\tau}' \cdot \mathbf{u}'(z=0), \quad (1)$$

where  $\boldsymbol{\tau}'$  is the near-inertial surface wind stress and  $\mathbf{u}'(z=0)$  is the horizontal baroclinic near-inertial velocity vector at the surface.

The depth-integrated near-inertial kinetic energy,  $KE$  is calculated following (Raja et al., 2022) as

$$KE = \frac{1}{2} \rho_0 \int_{-H}^0 |\mathbf{u}'|^2 dz, \quad (2)$$

and the depth integrated NIW energy fluxes in the horizontal are calculated as

$$\mathbf{F}_H = \int_{-H}^0 p' \mathbf{u}' dz, \quad (3)$$

where  $H$  is the seafloor depth,  $\rho_0$  is the reference density, and the near-inertial pressure perturbation,  $p'$ , is computed using the density anomaly,  $\rho'$ , as in Nash et al. (2005).

The three-dimensional HYCOM fields are also decomposed into vertical normal modes (Kelly, 2016; Buijsman et al., 2020). We adopt the same modal decomposition diagnostics used in Raja et al. (2022). The hydrostatic Sturm–Liouville equation is solved for non-equidistant HYCOM layers using 30-day mean profiles of buoyancy frequency in each horizontal grid cell, to obtain the velocity eigenfunctions. The horizontal velocity eigenfunctions,  $\mathcal{U}_n$ , are projected onto the vertical profiles of the horizontal baroclinic velocities,  $u$ , at every time step to yield the modal amplitudes in each horizontal grid cell, i.e.,

$$\hat{u}_n(t) = \frac{1}{H} \int_{-H}^0 \mathcal{U}_n(z) u(z, t) dz, \quad (4)$$

where  $\hat{u}_n$  is the modal amplitude of  $n$ th mode.

## 3. Spurious waves in global HYCOM simulations with DA

### 3.1. Model adjustment problem

During each DA cycle, the model variables are updated with corrections calculated by the DA system. The effect of these updates on the model output can be visualized using the time series of density contours from simulations with and without DA (Figs. 1a and b, respectively). The density contours are shown at a location in the North Atlantic ocean ( $40.3^\circ$  N,  $302.5^\circ$  W). We show the density contours for the upper 2000 m of the water column (the total depth at the location is 5162 m). In Fig. 1a, the insertion of corrections during DA causes shocks in the positioning of the isopycnals in the water column. The shocks are particularly severe on days corresponding to the availability

of observational data (predominantly from satellite altimetry) at the location.

In addition to abrupt displacement of isopycnals, the insertion of corrections also forces the model out of its dynamic balance. We quantify the dynamic imbalance introduced by DA in the global ocean using the thermal wind relations, which can be written as (Vallis, 2017)

$$-f \frac{\partial v}{\partial p} + \frac{1}{\rho^2} \frac{\partial \rho}{\partial x} = R_x, \quad (5)$$

$$-f \frac{\partial u}{\partial p} - \frac{1}{\rho^2} \frac{\partial \rho}{\partial y} = R_y, \quad (6)$$

where  $u$  and  $v$  are the horizontal velocities,  $p$  is the pressure,  $\rho$  is the density, and  $f$  is the Coriolis frequency. The residual terms,  $R_x$  and  $R_y$ , in Eqs. (5) and (6) are the measures of thermal wind imbalance. We calculate the thermal wind imbalances of the background and analysis fields from NCODA, and evaluate the imbalance generated during the insertion of corrections as the difference of residuals of the background and analysis fields.

The root-mean-square of the depth-integrated imbalances generated during the insertion of corrections along the  $x$  and  $y$  axes are shown in Fig. 2a and b, respectively. The imbalances are higher in the western boundary current regions and the Southern Ocean. These are regions of high mesoscale variability, where we expect frequent corrections to the model from the DA system (NCODA) in order to accurately capture the positions of the mesoscale eddies. Our finding implies that the geostrophic coupling within NCODA does not maintain the thermal wind balance very well.

The thermal wind balance does not apply near the equator because the Coriolis force goes to zero there. In the equatorial region, the dominant dynamic balance is between the ocean pressure gradients and the applied wind stress near the surface. The insertion of DA corrections can disrupt this balance near the equator, and trigger spurious vertical velocities and equatorial waves. Waters et al. (2017) discusses this type of model imbalance and proposes a modified bias pressure correction method to reduce the spurious vertical velocities near the equator. We focus on the DA induced dynamic imbalances that can lead to the generation of propagating near-inertial waves, away from the equator.

The dynamic imbalance generated during the insertion of corrections is also associated with a change in the gravitational potential energy ( $E_g$ ) of the water column when the depths of the isopycnals are adjusted by the DA correction. We evaluate the depth-integrated, volume averaged  $E_g$  following (Butler et al., 2013) as  $E_g = \int_{-H}^0 \rho g z dz$ , where  $g$  is the acceleration due to gravity and  $H$  is the depth of the ocean floor. The change in  $E_g$  during the daily update in EXPT 21.6,  $\Delta E_g$ , is calculated as the difference between  $E_g$  before and after the insertion of corrections in the model. We also compute  $\Delta E_g$  in the forward simulation (EXPT 19.0) over the time duration corresponding to the update time in EXPT 21.6, for comparison.

The root-mean-square  $\Delta E_g$  values for the simulation with and without DA are shown in Figs. 3a and b, respectively. The regions with high  $\Delta E_g$  in EXPT 21.6 correspond with the regions with enhanced thermal wind imbalance, in particular the western boundary current regions and the Southern Ocean (compare Fig. 3a with Fig. 2). The  $\Delta E_g$  is also enhanced along many internal tide beams in both simulations (Figs. 3a and b). This enhanced  $\Delta E_g$  is associated with the aliasing of diurnal and semi-diurnal internal tides and the super-tidal internal gravity waves (e.g., see Figure 16 of Savage et al., 2017b). The values of  $\Delta E_g$  are also elevated in the North Pacific in both simulations. This might be due to thermobaric instability (TBI), a numerical instability in HYCOM, due to imperfect compensation for compressibility in the pressure gradient term (Buijsman et al., 2016, 2020; Raja et al., 2022). The area identified to have TBI is enclosed by a blue dotted polygon in Fig. 3.

During the update, potential energy is injected into the ocean. This artificial source of energy drives the model adjustment process to regain the dynamic balance. The process of adjustment may involve the

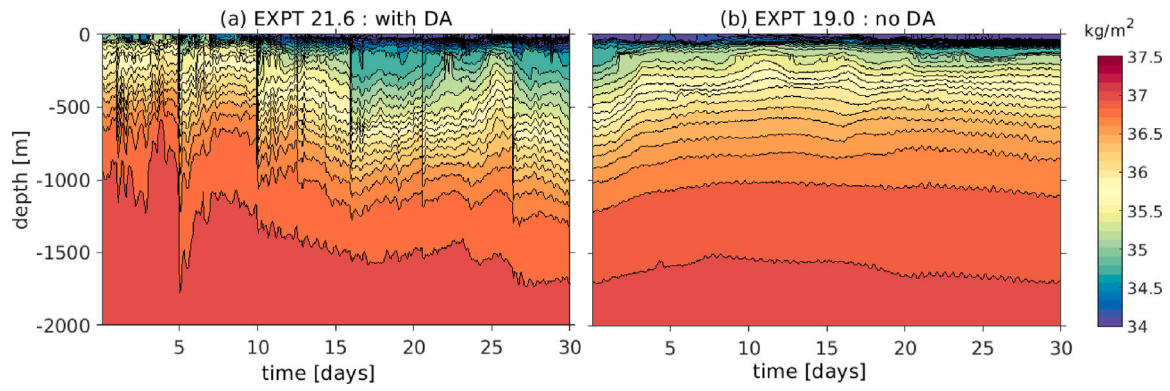


Fig. 1. Time series of density contours for a vertical profile in the Gulfstream at 40.3° N, 302.5° W for (a) EXPT 21.6 (with DA) and (b) EXPT 19.0 (no DA). The time series is shown for the top 2000 m. The total seafloor depth at the location is 5162 m.

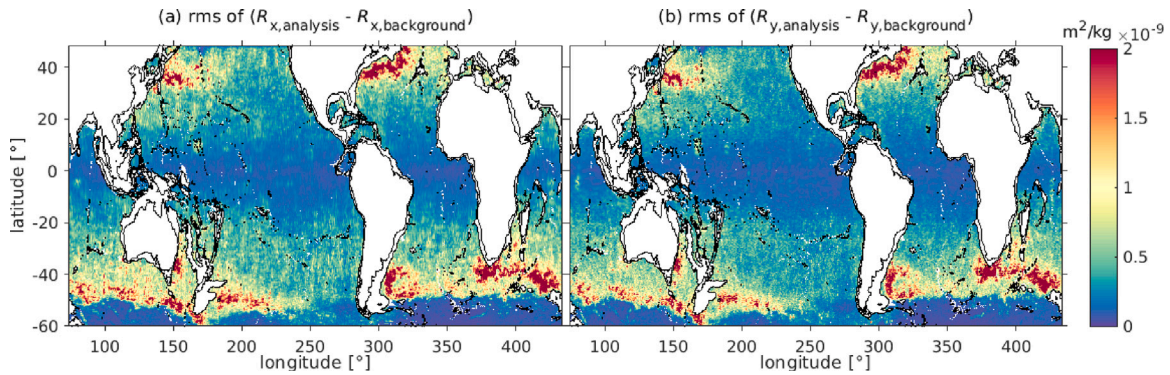


Fig. 2. Root-mean-square of the depth integrated thermal wind imbalance generated during DA updates, calculated as (a)  $R_{x,analysis} - R_{x,background}$ , and (b)  $R_{y,analysis} - R_{y,background}$  for 30 days in EXPT 21.6.

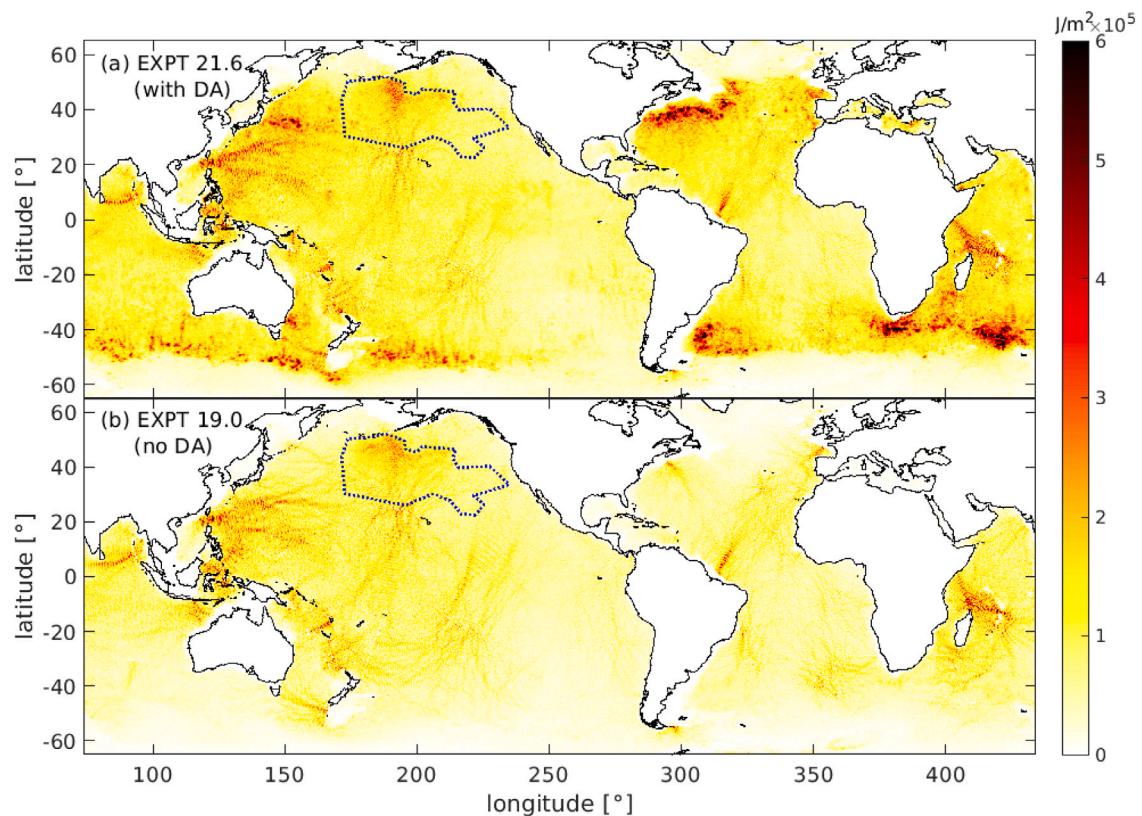


Fig. 3. Root-mean-square  $\Delta E_g$  in (a) EXPT 21.6 (with DA) and (b) EXPT 19.0 (No DA). The area enclosed by the blue dotted polygon is the region with TBI.

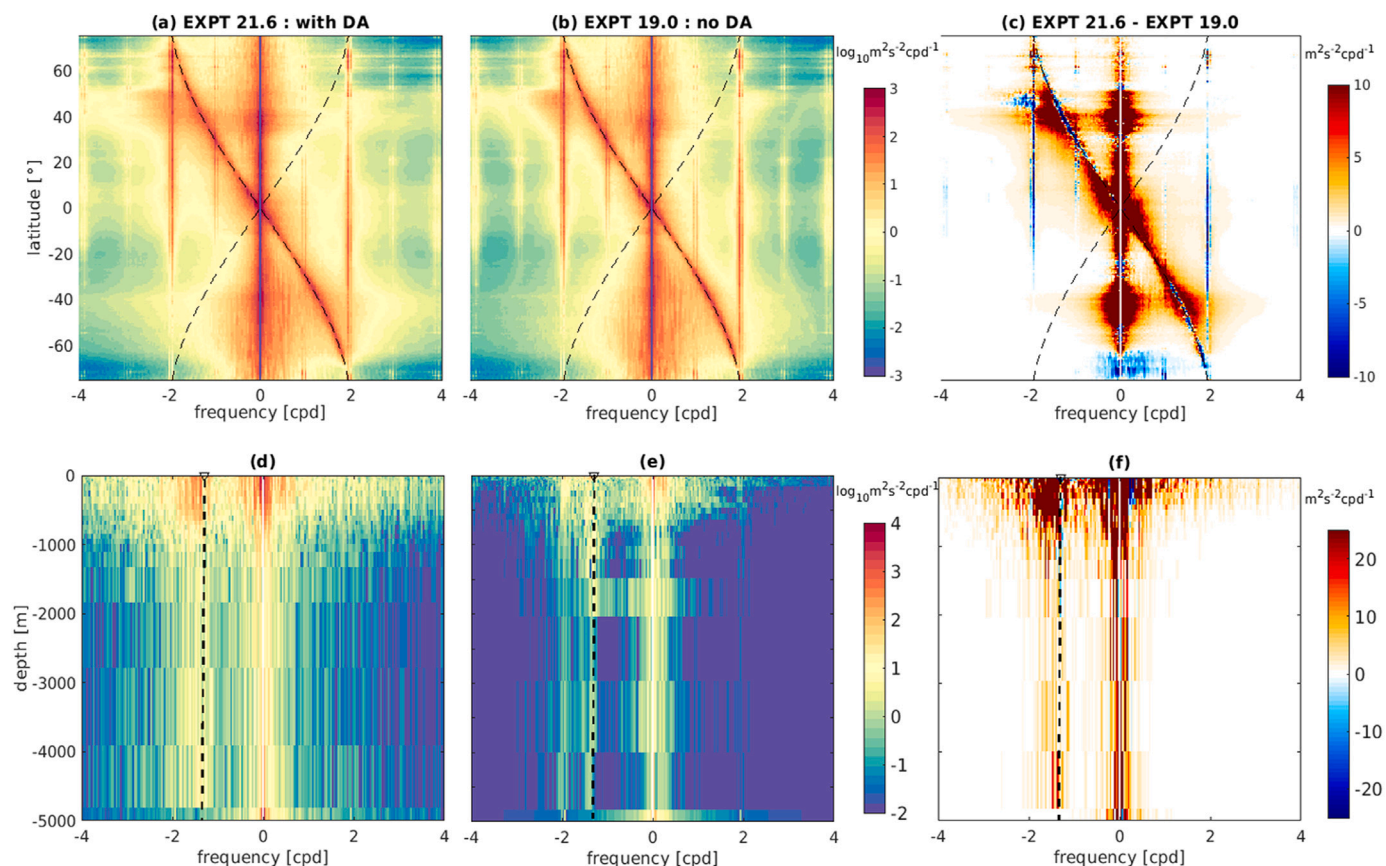


Fig. 4. Zonally averaged surface velocity rotary spectra in (a) EXPT 21.6 (with DA) and (b) EXPT 19.0 (no DA). (c) The difference of spectral densities between EXPT 21.6 and EXPT 19.0. The dashed curves indicate the Coriolis frequency,  $f$ . Velocity rotary spectra with depth at  $40.3^\circ$  N,  $302.5^\circ$  W in the Gulfstream in (d) EXPT 21.6 and (e) EXPT 19.0. (f) The difference of spectral densities between EXPT 21.6 and EXPT 19.0. The black dashed line indicates the local Coriolis frequency,  $f$ .

generation of spurious inertial oscillations and high-frequency internal gravity waves. In order to understand the spurious motions generated during model adjustment in detail, we examine the velocity rotary spectra in the simulations with and without DA.

The zonally averaged surface velocity rotary spectra as a function of frequency and latitude for EXPT 21.6 and EXPT 19.0 are shown in Fig. 4a and b, respectively. The spectra in both simulations are characterized by high-energy peaks at sub-tidal/low frequencies ( $< 0.5$  cpd) and diurnal, semidiurnal, and latitude-varying near-inertial frequencies. The difference in the spectral densities between the two experiments is shown in Fig. 4c. The simulation with DA (EXPT 21.6) has more energy concentrated in the sub-tidal frequencies and the near-inertial frequencies. We attribute the additional energy in the sub-tidal frequencies to the DA induced corrections to the placement of mesoscale eddies. In the near-inertial frequencies, it is due to the excitation of spurious NIWs when the DA increments adjust to the background field. We refer to this additional near-inertial energy as “spurious” because the wind forcing is the same for both simulations and NIWs in the ocean are predominantly excited through high-frequency winds resonantly interacting with surface ocean currents (Alford et al., 2016). We also calculate the near-inertial wind input (power transferred from wind to surface near-inertial motions) in simulations with and without DA, and found a variance of only 0.2%, thus proving that the additional NIW energy in the assimilative simulation is due to DA induced perturbations.

In Figs. 4d and e, we present a depth profile of the velocity rotary spectra in the Gulfstream region at  $40.3^\circ$  N,  $302.5^\circ$  W (at the same location of the density timeseries shown in Fig. 1) for EXPT 21.6 and EXPT 19.0, respectively. The spectra for both simulations show peaks of energy at the sub-tidal frequencies, semidiurnal and near-inertial frequencies. The difference of the spectra between the two

experiments (Fig. 4f) shows that the simulation with DA has more energy concentrated in the sub-tidal and the near-inertial frequencies. Notably, the spurious near-inertial energy is present throughout the water column even though most of it is in the upper 1000 m.

### 3.2. Spurious near-inertial waves

The energy in the simulation with DA in the sub-tidal frequencies (seen in the rotary spectra in Fig. 4) is associated with local processes that do not propagate horizontally from their generation sites. In contrast, the spurious energy in the near-inertial frequencies excites spurious near-inertial waves below the mixed layer that can propagate horizontally and mostly equatorward. We filter the model output fields in the near-inertial frequency range (as explained in Section 2.2.2) to analyze and characterize the spurious near-inertial motions in the assimilative simulation.

The depth-integrated, time-mean NIW kinetic energy for EXPT 21.6 (with DA) and EXPT 19.0 (no DA) are shown in Figs. 5a and b. Most of the NIW kinetic energy in both simulations resides in the Southern ocean. There is also enhanced NIW kinetic energy in the western boundary current regions ( $\sim 40^\circ$  N) in both experiments. The difference of NIW kinetic energy between the simulation with and without DA (i.e.,  $KE_{\text{EXPT 21.6}} - KE_{\text{EXPT 19.0}}$ ) is shown in Fig. 5c. EXPT 21.6 has more NIW KE in most of the ocean in general, with particularly enhanced KE in the Southern ocean and western boundary current regions. The zonally averaged near-inertial kinetic energy for the 2 experiments is presented in Fig. 5d. We find that with DA, EXPT 21.6 has 68% ( $\frac{300 \text{ PJ} - 178 \text{ PJ}}{178 \text{ PJ}}$ ) more NIW kinetic energy than EXPT 19.0, for the same wind forcing. EXPT 21.6 has higher energy in general throughout the global ocean but the energy is highest in regions with strong mesoscale

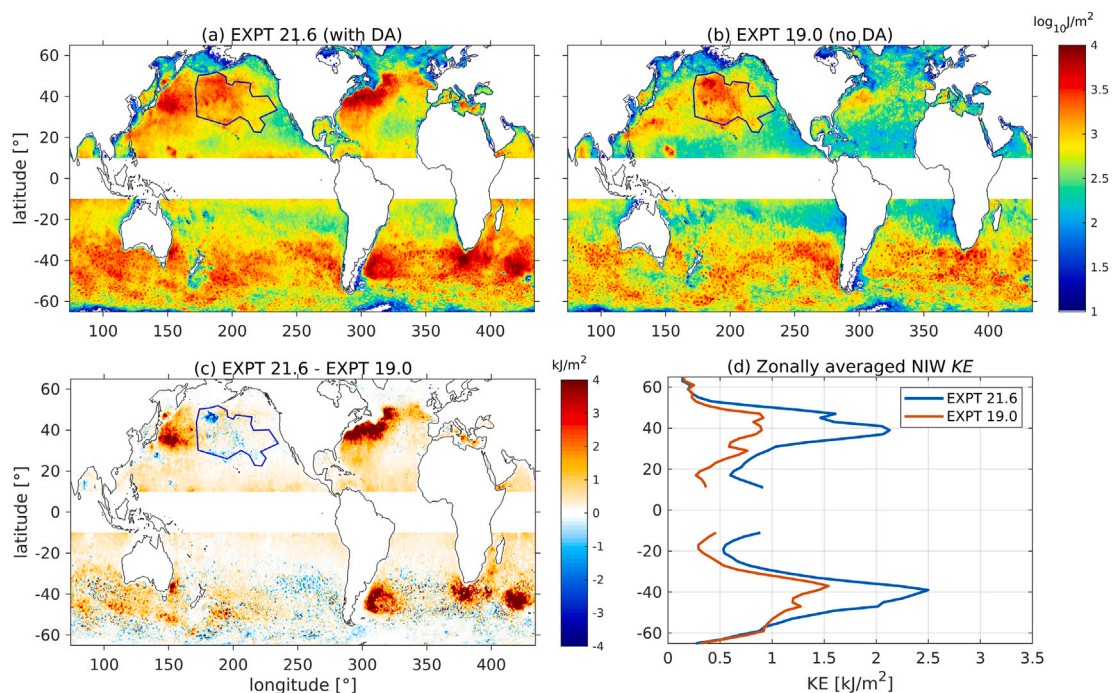


Fig. 5. Depth-integrated, time-mean NIW kinetic energy ( $KE$ ) for (a) EXPT 21.6 (with DA) and (b) EXPT 19.0 (no DA). (c) The difference of NIW  $KE$  between EXPT 21.6 and EXPT 19.0. (d) The zonally averaged NIW  $KE$  for EXPT 21.6 and EXPT 19.0. The area enclosed by the blue polygon are regions with TBI and are excluded from analysis.

variability. In these regions, the amplitude of the DA increments is large in order to correctly position the mesoscale features in the analysis fields (Figs. 2 and 3).

In order to understand the horizontal propagation of NIWs in the simulations with and without DA, we evaluate the horizontal energy fluxes as described in Section 2.2.2. The depth-integrated, time-mean NIW horizontal energy fluxes ( $F_H$ ) for EXPT 21.6 (with DA) and EXPT 19.0 (No DA) are presented in Figs. 6a and b (vectors), respectively. The time-mean near-inertial wind power input is shown in color in both figures. In Fig. 6a (EXPT 21.6), strong near-inertial fluxes are generated in regions with high mesoscale activity, particularly in the western boundary current regions. The generated fluxes occur in all directions, including poleward, indicating that these fluxes are due to waves with super-inertial frequencies. In Fig. 6b (EXPT 19.0), near-inertial fluxes are directed towards the equator from regions of high wind input in both hemispheres. The NIW energy fluxes are the strongest in the southeast Pacific (around 500 W/m) and the Southern Ocean (around 300 W/m) where the wind input is large. Strong northward and diverging fluxes occur in the northern Pacific south of the Aleutian islands in Fig. 6a and b without any corresponding wind power input. These fluxes might be due to TBI, as discussed in Buijsman et al. (2020). The broad-band disturbances associated with the TBI also have super-inertial frequencies that allow for poleward propagation.

The spurious NIW fluxes in the assimilative simulation propagate long distances equatorward from their generation sites in the extratropics. What modal structures do these waves have in order to persist such long journey without dissipation? In order to answer this question, we decompose the baroclinic fields into vertical normal modes. The horizontal resolution of our model ( $1/25^\circ$ ; 4 km near the equator) allows the first 5 semi-diurnal and near-inertial vertical modes to be resolved in most of the ocean (Buijsman et al., 2020; Raja et al., 2022).

The zonally averaged rotary spectra computed from the modal amplitudes of horizontal baroclinic velocity (Eq. (4)) for the simulation with DA, without DA, and their difference are shown in Fig. 7. The difference of rotary spectra of the two experiments shows that the

spurious near-inertial energy mostly projects on mode 1 (Fig. 7c). The results presented in Raja et al. (2022) show that the mode 1 NIWs propagate with group speeds close to 1 m/s and reach distances of  $\sim 1500$  km from their generation sites before they dissipate. Therefore, the spurious NIWs generated in the simulation with DA persist for a long time and propagate long distances horizontally. These propagating spurious NIWs may also interact with other small-scale, high-frequency motions and affect the energetics throughout the ocean basin.

#### 4. Effect of extended IAU periods on spurious internal waves

In this section, we analyze the role of the IAU period in suppressing the generation of spurious NIWs during DA. Bloom et al. (1996) introduced the IAU method as an initialization procedure to minimize the excitation of inertial motions during DA updates. Using a linear analysis of the IAU procedure, Bloom et al. (1996) demonstrate that it has the desired property of a low-pass time filter on the analysis fields following an update. The IAU procedure filters out the spurious motions with time periods less than the IAU period. In our analyses of the global simulation with DA, where the IAU period is 3 h, we find spurious near-inertial waves, which have time periods  $> 3$  hours in the global ocean, generated following the DA update. This implies that 3 h IAU is too short to prevent the generation of spurious high-frequency motions. Hence, we evaluate simulations with longer IAU periods to analyze the effect of extended IAU periods on spurious NIWs.

In order to study the role of the IAU period in the generation of spurious NIWs, we establish a test-bed using HYCOM simulations in an existing regional configuration of the Gulf of Mexico (Dukhovskoy et al., 2015). The Gulf of Mexico region is also chosen because it has relatively weak internal tides, strong surface winds and a dynamic mesoscale field. The simulations are run with  $1/25^\circ$  horizontal spatial resolution and 41 vertical layers, similar to the global model simulations. Since the Navy's NCODA system is proprietary and not publicly available, we use the open-source data assimilation package, Tendral Statistical Interpolation System (TSIS), developed by Srinivasan

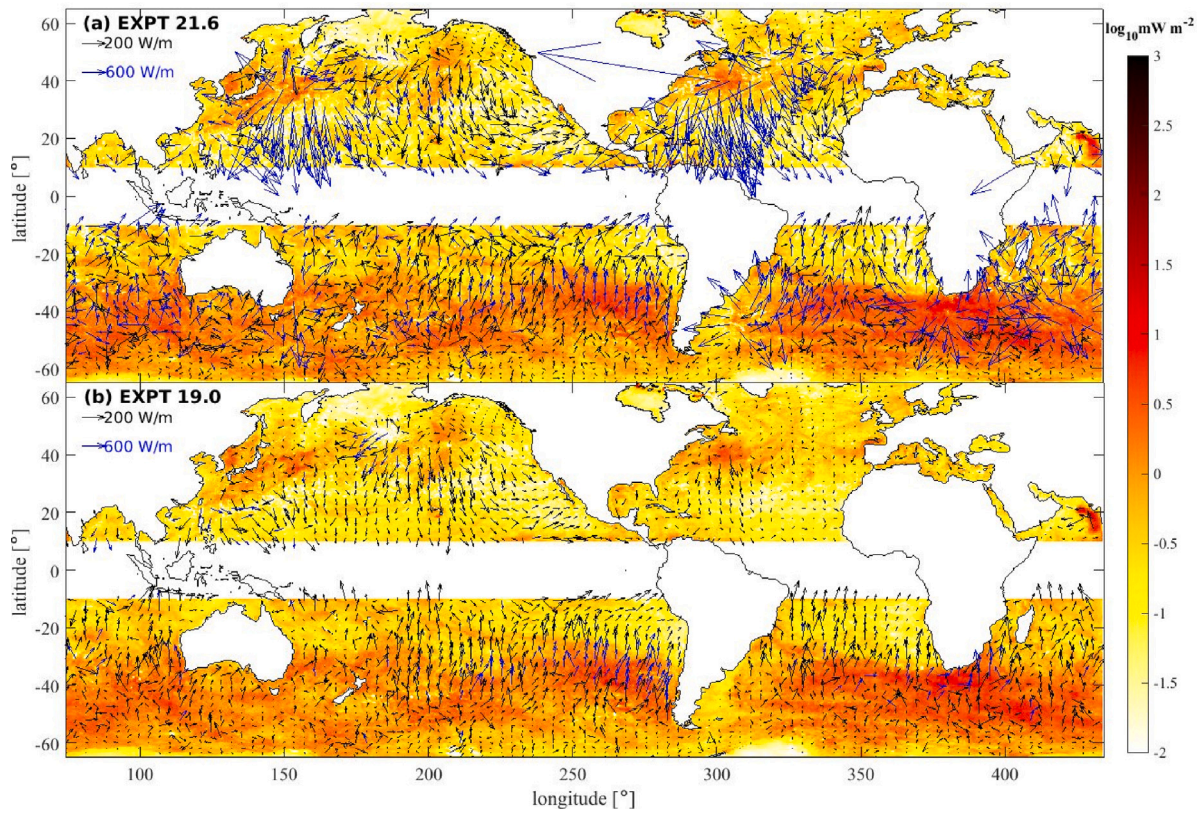


Fig. 6. Time-mean near-inertial surface wind power input ( $W$ ; color), and depth-integrated NIW horizontal energy flux (vectors) for (a) EXPT 21.6 and (b) EXPT 19.0. The black vectors represent fluxes with a magnitude less than 100 W/m and the blue vectors represent fluxes with a magnitude larger than 100 W/m.

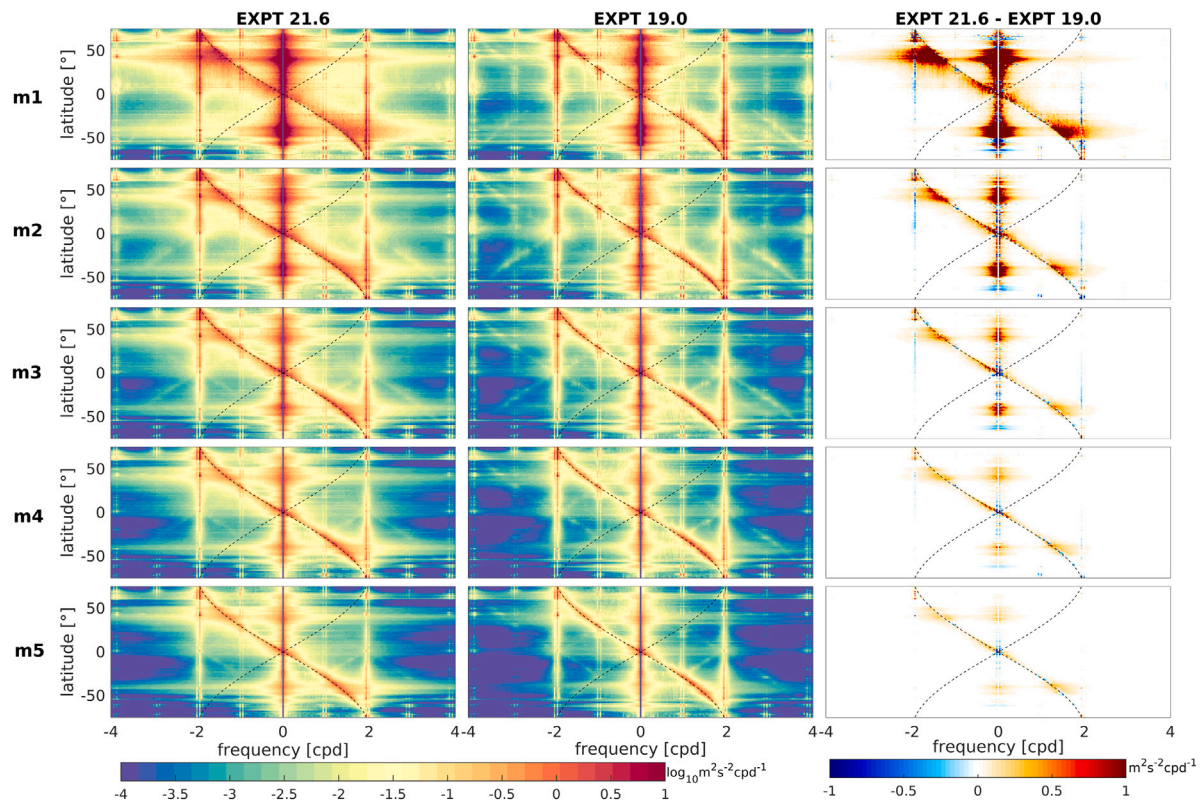
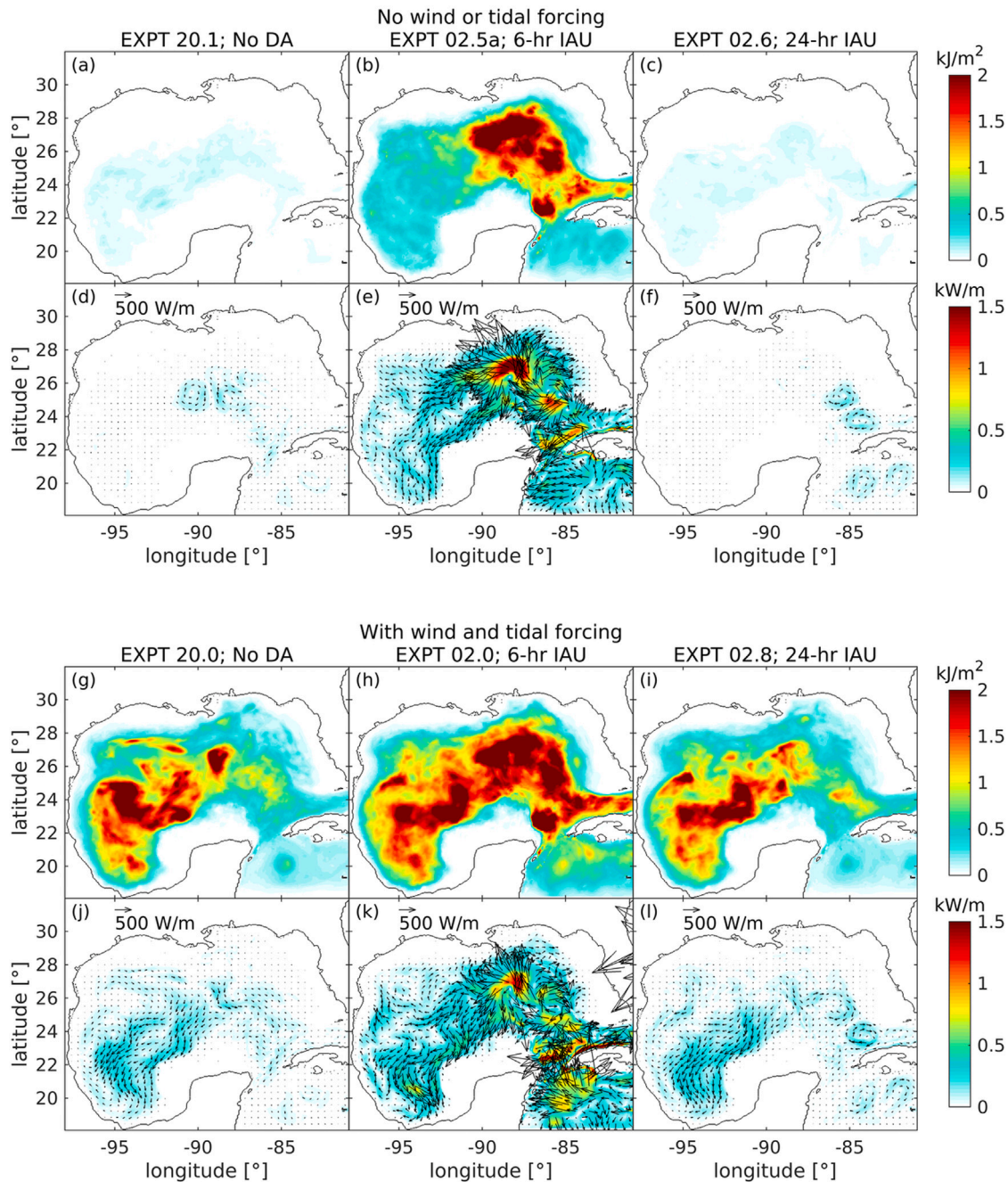


Fig. 7. Zonally averaged velocity rotary spectra of modal amplitudes for modes 1 to 5 for EXPT 21.6 (first column), EXPT 19.0 (second column), and their differences (third column).



**Fig. 8.** The depth-integrated, time-mean NIW kinetic energy in the Gulf of Mexico in simulations without wind and tidal forcing with (a) no DA, (b) 6 h IAU, and (c) 24 h IAU. The depth-integrated, time-mean NIW horizontal energy fluxes (vectors) and NIW flux amplitudes (color) in simulations without wind and tidal forcing with (d) no DA, (e) 6 h IAU, and (f) 24 h IAU. (g–l) are the same as (a–f), but for the addition of wind and tidal forcing.

et al. (2022), to assimilate observational data in the regional model as in Dukhovskoy et al. (2023). In these regional simulations, we refrain from geostrophically coupling the data-derived increments, as this approach allows us to isolate and investigate the specific impact of the IAU period on spurious NIWs. The simulations have realistic atmospheric forcing from the Climate Forecast System Version 2 (CFSv2), developed by the National Centers for Environmental Prediction (NCEP) (Saha et al., 2014), with  $0.205^\circ$  horizontal resolution and hourly forcing frequency.

We first analyze the spurious NIWs in isolation from the physical internal waves in the region by running an assimilative simulation without the wind and tidal forcing. We then test different IAU periods

and examine the effect of IAU period on the generation of spurious NIWs in the model. The assimilative simulations are compared against a parallel forward simulation. The same set of simulations are then repeated with the addition of wind and tidal forcing to confirm that changing the IAU period does not affect the physical internal waves in the region. We test IAU periods of 6, 12, 18 and 24 h. The list of regional simulations and their descriptions are shown in Table 1.

The time-mean, depth-integrated NIW kinetic energy and NIW energy fluxes for simulations without wind and tidal forcing are shown in Fig. 8a–f. The forward simulation without DA (Figs. 8a and d) shows no presence of near-inertial motions. When the IAU period is 6 h (Figs. 8b and e), the DA generates spurious waves in broad near-inertial



**Table 1**  
List of the regional HYCOM simulations of the Gulf of Mexico.

| EXPT  | Assimilation ( $T_{IAU}$ , if any) | Tidal forcing | Wind forcing |
|-------|------------------------------------|---------------|--------------|
| 20.1  | No DA                              | No            | No           |
| 02.5a | TSIS (6 h)                         | No            | No           |
| 02.5b | TSIS (12 h)                        | No            | No           |
| 02.5c | TSIS (18 h)                        | No            | No           |
| 02.6  | TSIS (24 h)                        | No            | No           |
| 20.0  | No DA                              | Yes           | Yes          |
| 02.0  | TSIS (6 h)                         | Yes           | Yes          |
| 02.3  | TSIS (12 h)                        | Yes           | Yes          |
| 02.7  | TSIS (18 h)                        | Yes           | Yes          |
| 02.8  | TSIS (24 h)                        | Yes           | Yes          |

frequency band that diverge from a region south of the Mississippi coast. When the IAU period is extended to 24 h (Figs. 8c and f), the kinetic energy associated with the spurious NIWs is greatly diminished.

Figs. 8g–i show the time-mean, depth-integrated NIW kinetic energy and NIW energy fluxes for simulations with wind and tidal forcing. This time in the forward simulation (Figs. 8g and j), the wind-generated NIWs are present in the western Gulf of Mexico. In the assimilative simulation with 6 h IAU period (Figs. 8h and k), the spurious NIWs present mostly in the eastern Gulf of Mexico dominate the wind-generated NIWs. These spurious NIWs are due to large DA corrections in the loop current region. When the IAU period is increased to 24 h, the spurious NIWs are minimal, and the NIW kinetic energy and fluxes in Figs. 8i and l compare well with those of the forward simulation (Figs. 8g and j).

Fig. 9a summarizes the depth and area integrated NIW kinetic energy in the Gulf of Mexico for all the regional simulations listed in Table 1. In the experiments with and without wind and tidal forcing, the NIW kinetic energy decreases with increasing IAU period, and the simulations with 24 h IAU period have almost the same value of NIW  $KE$  as the forward simulations.

## 5. Summary and discussion

The primary purpose of this paper is to investigate the spurious high frequency waves generated by the NCODA DA procedure in the Navy's ocean forecast system. Using the analysis presented here, we show that the current implementation of DA in HYCOM introduces spurious NIWs that can overshadow the generation and propagation of the physical internal waves in the model. These spurious waves contaminate the short-range forecast that provides the background state for the next analysis, adding to the difficulty of extracting useful information from the observation data (Ourmieres et al., 2006). Although this may have little impact on the large-scale mesoscale circulation, it does affect small-scale/high-frequency ocean dynamics, especially in high-resolution simulations that do resolve these scales. Our main conclusions from this study are:

1. The current implementation of data assimilation in the US Navy's operational global ocean prediction system generates spurious NIWs during updates. The 3 h IAU period used in the Navy's ocean forecast systems (GOFS 3.5, and the soon-to-be operational ESPC) is not sufficient to eliminate these spurious NIWs in the analysis fields.
2. The spurious NIWs mostly project on low baroclinic modes that propagate long horizontal distances from their generation sites. The presence of these spurious waves makes the model simulations very difficult to use for the study of small-scale/high-frequency motions.
3. Increasing the duration of IAU period to 24 h results in the reduction of spurious NIW generation. The variance of near-inertial kinetic energy between the assimilative and forward simulations is reduced to  $\sim 1\%$  with a 24 h IAU period.

The past studies on the impact of DA induced model adjustments and their consequences have mainly focused only on the accuracy of mesoscale eddies in the forecast fields, and not explicitly on the quality of the fields in terms of high-frequency/small-scale motions. Bell et al. (2004) discuss how the incorporation of thermal data into an ocean model near the equator frequently leads to a dynamically unbalanced state with unrealistic deep overturning circulations in the equatorial region. More recently, Pilo et al. (2018) discuss the impact of DA on vertical velocities (chosen because of their sensitivity to model dynamic balances) within mesoscale eddies in the subtropics. They find that the model adjustment following the insertion of increments distorts the eddies on the first day after assimilation, and suggest that the model fields from the first day after assimilation should be disregarded. However, our study shows that the low-mode NIWs generated as a consequence of the DA induced model adjustment are persistent and propagate long distances from their generation sites. These spurious NIWs are capable of disrupting the high-frequency dynamics in short-medium range forecasts.

The importance of accurate representation of internal wave dynamics in the global ocean models has been widely reported in the past (e.g., Arbic et al., 2010; Simmons and Alford, 2012; Buijsman et al., 2020; Raja et al., 2022; Arbic et al., 2022). Recently, as the spatial resolution of the ocean forecast systems increases, the need for simulations of global ocean models that simultaneously include realistic atmospheric and tidal forcing have grown (Arbic, 2022). The prediction of internal tide amplitude and phase (especially that of the non-phase-locked internal tides) require accurate forecasts of the mesoscale eddies and time-varying stratification (Shriver et al., 2012; Luecke et al., 2020). This demand for assimilative simulations that can accurately represent internal tides will likely increase further as the next generation altimeter missions such as the Surface Water Ocean Topography (SWOT) mission come online and require precise corrections of the high-frequency internal wave motions.

Moreover, global ocean models with DA such as operational HYCOM, are often used for the initialization of various regional models (Prasad and Hogan, 2007; Barth et al., 2008). These nested regional models with very high spatial resolutions are used for studying ocean processes of short length and time scales because the global HYCOM does not sufficiently resolve such detailed physics due to its coarser grid resolution. The remotely generated internal waves can affect the energetics in the regional simulations as they propagate into the nested domain and dissipate there (Nelson et al., 2020; Siyanbola et al., 2023). Hence, it is crucial to improve the representation of internal waves in assimilative ocean model simulations.

In our analyses, we demonstrate that the generation of spurious NIWs during DA is minimized in simulations with a longer IAU period than the typical 3 h IAU used in Navy's ocean forecast systems. Without wind and tidal forcing (blue line in Fig. 9a), when the IAU period is 6 h, the spurious near-inertial energy is as much as the near-inertial energy in the forward simulation with wind and tidal forcing (red line Fig. 9a). Increasing the IAU period decreases the spurious NIW energy, and with a 24 h IAU period, we find that the assimilative simulations have the same NIW energy as the forward simulation (implying that all the spurious waves are removed with the 24 h IAU).

When discussing the IAU technique, Bloom et al. (1996) conduct a comparison of various methods for introducing the analysis increment into a linear oscillator characterized by complex frequencies. They contrast the IAU method with direct insertion of the analysis increment and demonstrate that, unlike direct insertion, which maintains a constant response amplitude regardless of frequency, IAU induces a diminishing amplitude in the response of a neutral oscillator as the frequency increases. In simpler terms, the IAU process functions akin to a low-pass filter on the analysis fields, reducing high-frequency motions generated by data assimilation, particularly those with time periods shorter than the IAU period. In Fig. 9b, we present the amplitude of the IAU response function, as per the calculations outlined by Bloom et al.

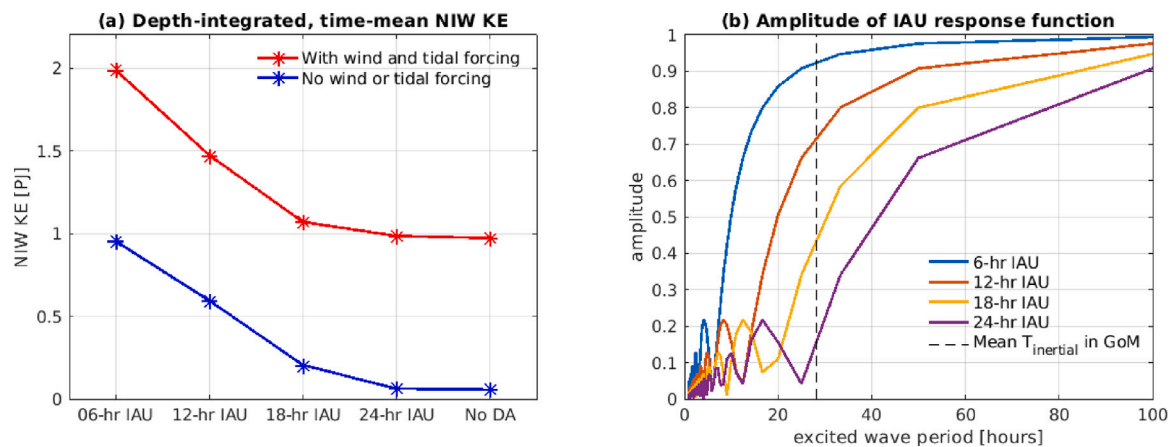


Fig. 9. (a) Depth-integrated, time-mean NIW kinetic energy in the Gulf of Mexico regional simulations with IAU periods of 6, 12, 18 and 24 h. (b) The amplitude of the IAU response function (calculated according to Bloom et al. (1996)) for the same IAU periods with respect to the excited wave periods. The black dashed line shows the mean inertial period in the Gulf of Mexico.

(1996), for the different IAU periods tested in our study. Notably, the response function reveals the attenuation of spurious motions resulting from the insertion of increments with wave periods shorter than the chosen IAU period.

Our analyses in the context of Bloom et al. (1996) imply that the duration of the IAU period should be longer than the local inertial period, in order to effectively minimize the generation of spurious NIWs. This is not practically possible to implement since the inertial period increases to infinity as the latitude decreases in the global ocean. However, from the global map of spurious NIW kinetic energy (Fig. 5c), we see that the spurious NIWs are excited mostly in the mid-latitudes. Therefore, increasing the IAU period to 24 h will diminish the generation of spurious NIWs in most of the ocean (poleward of  $\sim 30^\circ$ ). We will test this hypothesis using a global HYCOM simulation with 24 h IAU period in a future paper.

Finally, it is important to acknowledge that employing an extended IAU period (e.g., 24 h) does not solve the dynamic imbalance during the insertion of increments, but serves only as a provisional measure in mitigating the generation of persistent spurious internal waves within assimilative models. However, for a sustainable resolution of this problem, a comprehensive reformulation of the DA system is needed. We postulate that the adoption of a generalized 4-dimensional variational (4DVAR) scheme or a Local Ensemble Transform Kalman Filter (LETKF; Hunt et al., 2007), holds the potential to yield significantly better analyses and forecasts of the ocean state compared to the prevalent 3DVAR approach. This improvement is primarily attributed to the better handling of time-dependent observations and allowing for the propagation of information from observation sites to all other model variables in a dynamically consistent manner. This stands in contrast to the current 3DVAR method, which relies on predetermined static covariances. Future efforts will concentrate on the implementation of these capabilities into the HYCOM forecasting system.

#### CRedit authorship contribution statement

**Keshav J. Raja:** Conceptualization, Formal analysis, Investigation, Methodology, Software, Visualization, Writing – original draft, Writing – review & editing. **Maarten C. Buijsman:** Conceptualization, Formal analysis, Funding acquisition, Methodology, Resources, Software, Supervision, Writing – review & editing. **Alexandra Bozec:** Methodology, Software. **Robert W. Helber:** Formal analysis, Methodology, Software, Writing – review & editing. **Jay F. Shriver:** Methodology, Software. **Alan Wallcraft:** Methodology, Software, Writing – review & editing. **Eric P. Chassignet:** Conceptualization, Funding acquisition, Resources, Supervision, Writing – review & editing. **Brian K. Arbic:** Conceptualization, Writing – review & editing.

#### Declaration of competing interest

The authors declare that they have no known competing financial interests or personal relationships that could have appeared to influence the work reported in this paper.

#### Data availability

Data will be made available on request.

#### Acknowledgments

The initial part of this work was supported by the Office of Naval Research, United States of America through NISKINE project grants N00014-18-1-2801 (Raja and Buijsman), N00014-20-W-X01883 (Shriver), and N00014-18-1-2544 (Arbic). The study of the impact of IAU period using regional simulations was supported by the Office of Naval Research, United States of America through the NOPP Global Internal Waves grant N00014-22-S-B003 (Chassignet, Raja, Bozec, and Wallcraft). We thank the two reviewers for their careful reading of the manuscript, and their helpful comments which improved the presentation of the article.

#### References

- Alford, M.H., MacKinnon, J.A., Simmons, H.L., Nash, J.D., 2016. Near-inertial internal gravity waves in the ocean. *Annu. Rev. Mar. Sci.* 8, 95–123.
- Arbic, B.K., 2022. Incorporating tides and internal gravity waves within global ocean general circulation models: A review. *Prog. Oceanogr.* 102824.
- Arbic, B.K., Alford, M.H., Ansong, J.K., Buijsman, M.C., Ciotti, R.B., Farrar, J.T., Hallberg, R.W., Henze, C.E., Hill, C.N., Luecke, C.A., et al., 2018. A primer on global internal tide and internal gravity wave continuum modeling in HYCOM and MITgcm. *New Front. Oper. Oceanogr.*
- Arbic, B.K., Elipot, S., Brasch, J.M., Menemenlis, D., Ponte, A.L., Shriver, J.F., Yu, X., Zaron, E.D., Alford, M.H., Buijsman, M.C., et al., 2022. Near-surface oceanic kinetic energy distributions from drifter observations and numerical models. *J. Geophys. Res.: Oceans* 127 (10), e2022JC018551.
- Arbic, B.K., Richman, J.G., Shriver, J.F., Timko, P.G., Metzger, E.J., Wallcraft, A.J., 2012. Global modeling of internal tides: Within an eddy ocean general circulation model. *Oceanography* 25 (2), 20–29.
- Arbic, B.K., Wallcraft, A.J., Metzger, E.J., 2010. Concurrent simulation of the eddy general circulation and tides in a global ocean model. *Ocean Model.* 32 (3–4), 175–187.
- Barth, A., Alvera-Azcárate, A., Weisberg, R.H., 2008. Assimilation of high-frequency radar currents in a nested model of the west florida shelf. *J. Geophys. Res.: Oceans* 113 (C8).
- Bell, M.J., Martin, M., Nichols, N., 2004. Assimilation of data into an ocean model with systematic errors near the equator. *Q. J. R. Meteorol. Soc.: A J. Atmospheric Sci., Appl. Meteorol. Phys. Oceanogr.* 130 (598), 873–893.

- Bleck, R., 2002. An oceanic general circulation model framed in hybrid isopycnic-cartesian coordinates. *Ocean Modell* 4 (1), 55–88.
- Bloom, S., Takacs, L., Da Silva, A., Ledvina, D., 1996. Data assimilation using incremental analysis updates. *Mon. Weather Rev.* 124 (6), 1256–1271.
- Buijsman, M.C., Ansong, J.K., Arbic, B.K., Richman, J.G., Shriver, J.F., Timko, P.G., Wallcraft, A.J., Whalen, C.B., Zhao, Z., 2016. Impact of parameterized internal wave drag on the semi-diurnal energy balance in a global ocean circulation model. *J. Phys. Oceanogr.* 46 (5), 1399–1419.
- Buijsman, M.C., Arbic, B.K., Richman, J.G., Shriver, J.F., Wallcraft, A.J., Zamudio, L., 2017. Semi-diurnal internal tide incoherence in the equatorial Pacific. *J. Geophys. Res.: Oceans* 122 (7), 5286–5305.
- Buijsman, M.C., Stephenson, G.R., Ansong, J.K., Arbic, B.K., Green, J.M., Richman, J.G., Shriver, J.F., Vic, C., Wallcraft, A.J., Zhao, Z., 2020. On the interplay between horizontal resolution and wave drag and their effect on tidal baroclinic mode waves in realistic global ocean simulations. *Ocean Model.* 152, 101656.
- Butler, E., Oliver, K., Gregory, J.M., Tailleux, R., 2013. The ocean's gravitational potential energy budget in a coupled climate model. *Geophys. Res. Lett.* 40 (20), 5417–5422.
- Chassignet, E.P., Hurlburt, H.E., Metzger, E.J., Smedstad, O.M., Cummings, J.A., Halliwell, G.R., Bleck, R., Baraille, R., Wallcraft, A.J., Lozano, C., et al., 2009. US GODAE: global ocean prediction with the hybrid coordinate ocean model (HYCOM). *Oceanography* 22 (2), 64–75.
- Chassignet, E.P., Smith, L.T., Halliwell, G.R., Bleck, R., 2003. North atlantic simulations with the hybrid coordinate ocean model (HYCOM): Impact of the vertical coordinate choice, reference pressure, and thermobaricity. *J. Phys. Oceanogr.* 33 (12), 2504–2526.
- Cummings, J.A., Peak, J.E., 2014. Validation test report for the variational assimilation of satellite sea surface temperature radiances. Naval Research Lab Stennis Detachment Stennis Space Center MS.
- Cummings, J.A., Smedstad, O.M., 2014. Ocean data impacts in global HYCOM. *J. Atmos. Ocean. Technol.* 31 (8), 1771–1791.
- Dukhovskoy, D.S., Chassignet, E.P., Bozec, A., Morey, S.L., 2023. Assessment of predictability of the loop current in the Gulf of Mexico from observing system experiments and observing system simulation experiments. *Front. Mar. Sci.*
- Dukhovskoy, D.S., Leben, R.R., Chassignet, E.P., Hall, C.A., Morey, S.L., Nedbor-Gross, R., 2015. Characterization of the uncertainty of loop current metrics using a multidecadal numerical simulation and altimeter observations. *Deep Sea Res. I: Oceanogr. Res. Pap.* 100, 140–158.
- Gasparin, F., Cravatte, S., Greiner, E., Perruche, C., Hamon, M., Van Gennip, S., Lellouche, J.-M., 2021. Excessive productivity and heat content in tropical Pacific analyses: disentangling the effects of in situ and altimetry assimilation. *Ocean Model.* 160, 101768.
- Gonella, J., 1972. A rotary-component method for analysing meteorological and oceanographic vector time series. In: *Deep Sea Research and Oceanographic Abstracts*. 19, (12), Elsevier, pp. 833–846.
- Hogan, T.F., Liu, M., Ridout, J.A., Peng, M.S., Whitcomb, T.R., Ruston, B.C., Reynolds, C.A., Eckermann, S.D., Moskaitis, J.R., Baker, N.L., et al., 2014. The navy global environmental model. *Oceanography* 27 (3), 116–125.
- Hunke, E.C., Lipscomb, W.H., 2008. The Los Alamos Sea Ice Model Documentation and Software User's Manual, Version 4.0. Tech Rep: LA-CC-06-012, Los Alamos National Laboratory.
- Hunt, B.R., Kostelich, E.J., Szunyogh, I., 2007. Efficient data assimilation for spatiotemporal chaos: A local ensemble transform Kalman filter. *Physica D* 230 (1–2), 112–126.
- Kelly, S.M., 2016. The vertical mode decomposition of surface and internal tides in the presence of a free surface and arbitrary topography. *J. Phys. Oceanogr.* 46 (12), 3777–3788.
- Lange, H., Craig, G.C., Janjić, T., 2017. Characterizing noise and spurious convection in convective data assimilation. *Q. J. R. Meteorol. Soc.* 143 (709), 3060–3069.
- Leaman, K.D., Sanford, T.B., 1975. Vertical energy propagation of inertial waves: A vector spectral analysis of velocity profiles. *J. Geophys. Res.* 80 (15), 1975–1978.
- Luecke, C.A., Arbic, B.K., Richman, J.G., Shriver, J.F., Alford, M.H., Ansong, J.K., Bassette, S.L., Buijsman, M.C., Menemenlis, D., Scott, R.B., et al., 2020. Statistical comparisons of temperature variance and kinetic energy in global ocean models and observations: Results from mesoscale to internal wave frequencies. *J. Geophys. Res.: Oceans* 125 (5), e2019JC015306.
- Metzger, E., Helber, R.W., Hogan, P.J., Posey, P.G., Thoppil, P.G., Townsend, T.L., Wallcraft, A.J., Smedstad, O.M., Franklin, D.S., Zamudo-Lopez, L., et al., 2017. Global ocean forecast system 3.1 validation test. In: Technical Report. Naval Research Lab Stennis Detachment Stennis Space Center MS Stennis Space ...
- Metzger, E., Hogan, P., Shriver, J., Thoppil, P., Douglass, E., Yu, Z., Allard, R., Rowley, C., Smedstad, O., Franklin, D., et al., 2020. Validation test report for the global ocean forecast system 3.5-1/25 degree hycom/cice with tides. In: Technical Report. NAVAL RESEARCH LAB WASHINGTON DC WASHINGTON United States.
- Morrow, R., Fu, L.-L., Arduin, F., Benkiran, M., Chapron, B., Cosme, E., d'Ovidio, F., Farrar, J.T., Gille, S.T., Lapeyre, G., et al., 2019. Global observations of fine-scale ocean surface topography with the surface water and ocean topography (SWOT) mission. *Front. Marine Sci.* 6, 232.
- Müller, M., Arbic, B.K., Richman, J.G., Shriver, J.F., Kunze, E.L., Scott, R.B., Wallcraft, A.J., Zamudio, L., 2015. Toward an internal gravity wave spectrum in global ocean models. *Geophys. Res. Lett.* 42 (9), 3474–3481.
- Nash, J.D., Alford, M.H., Kunze, E., 2005. Estimating internal wave energy fluxes in the ocean. *J. Atmos. Ocean. Technol.* 22 (10), 1551–1570.
- Nelson, A., Arbic, B., Menemenlis, D., Peltier, W., Alford, M., Grisouard, N., Klymak, J., 2020. Improved internal wave spectral continuum in a regional ocean model. *J. Geophys. Res.: Oceans* 125 (5), e2019JC015974.
- Nelson, A.D., Arbic, B.K., Zaron, E.D., Savage, A.C., Richman, J.G., Buijsman, M.C., Shriver, J.F., 2019. Toward realistic nonstationarity of semi-diurnal baroclinic tides in a hydrodynamic model. *J. Geophys. Res.: Oceans* 124 (9), 6632–6642.
- Ourmieres, Y., Brankart, J.-M., Berline, L., Brasseur, P., Verron, J., 2006. Incremental analysis update implementation into a sequential ocean data assimilation system. *J. Atmos. Ocean. Technol.* 23 (12), 1729–1744.
- Pilo, G.S., Oke, P.R., Coleman, R., Rykova, T., Ridgway, K., 2018. Impact of data assimilation on vertical velocities in an eddy resolving ocean model. *Ocean Model.* 131, 71–85.
- Prasad, T., Hogan, P.J., 2007. Upper-ocean response to Hurricane Ivan in a 1/25 nested Gulf of Mexico HYCOM. *J. Geophys. Res.: Oceans* 112 (C4).
- Raja, K.J., Buijsman, M.C., Shriver, J.F., Arbic, B.K., Siyanbola, O., 2022. Near-inertial wave energetics modulated by background flows in a global model simulation. *J. Phys. Oceanogr.* 52 (5), 823–840.
- Saha, S., Moorthi, S., Wu, X., Wang, J., Nadiga, S., Tripp, P., Behringer, D., Hou, Y.-T., Chuang, H.-y., Iredell, M., et al., 2014. The NCEP climate forecast system version 2. *J. Climate* 27 (6), 2185–2208.
- Savage, A.C., Arbic, B.K., Alford, M.H., Ansong, J.K., Farrar, J.T., Menemenlis, D., O'Rourke, A.K., Richman, J.G., Shriver, J.F., Voet, G., et al., 2017a. Spectral decomposition of internal gravity wave sea surface height in global models. *J. Geophys. Res.: Oceans* 122 (10), 7803–7821.
- Savage, A.C., Arbic, B.K., Richman, J.G., Shriver, J.F., Alford, M.H., Buijsman, M.C., Thomas Farrar, J., Sharma, H., Voet, G., Wallcraft, A.J., et al., 2017b. Frequency content of sea surface height variability from internal gravity waves to mesoscale eddies. *J. Geophys. Res.: Oceans* 122 (3), 2519–2538.
- Shriver, J., Arbic, B.K., Richman, J., Ray, R., Metzger, E., Wallcraft, A., Timko, P., 2012. An evaluation of the barotropic and internal tides in a high-resolution global ocean circulation model. *J. Geophys. Res.: Oceans* 117 (C10).
- Shriver, J.F., Richman, J.G., Arbic, B.K., 2014. How stationary are the internal tides in a high-resolution global ocean circulation model? *J. Geophys. Res.: Oceans* 119 (5), 2769–2787.
- Simmons, H.L., Alford, M.H., 2012. Simulating the long-range swell of internal waves generated by ocean storms. *Oceanography* 25 (2), 30–41.
- Siyanbola, O.Q., Buijsman, M.C., Delpach, A., Renault, L., Barkan, R., Shriver, J.F., Arbic, B.K., McWilliams, J.C., 2023. Remote internal wave forcing of regional ocean simulations near the US West Coast. *Ocean Model.* 181, 102154.
- Srinivasan, A., Chin, T., Chassignet, E., Iskandarani, M., Groves, N., 2022. A statistical interpolation code for ocean analysis and forecasting. *J. Atmos. Ocean. Technol.* 39 (3), 367–386.
- Thomson, R.E., Emery, W.J., 2014. *Data Analysis Methods in Physical Oceanography*. Newnes.
- Vallis, G.K., 2017. *Atmospheric and Oceanic Fluid Dynamics*. Cambridge University Press.
- Waters, J., Bell, M., Martin, M., Lea, D., 2017. Reducing ocean model imbalances in the equatorial region caused by data assimilation. *Q. J. R. Meteorol. Soc.* 143 (702), 195–208.
- Yu, X., Ponte, A.L., Elipot, S., Menemenlis, D., Zaron, E.D., Abernathy, R., 2019. Surface kinetic energy distributions in the global oceans from a high-resolution numerical model and surface drifter observations. *Geophys. Res. Lett.* 46 (16), 9757–9766.